Intertwined Van Hove Singularities as a Mechanism for Loop Current Order in Kagome Metals

Heqiu Li,[1] Yong Baek Kim,[1,2,*] and Hae-Young Kee[1,3,†]
[1]*Department of Physics, University of Toronto, Toronto, Ontario M5S 1A7, Canada*
[2]*School of Physics, Korea Institute for Advanced Study, Seoul 02455, Korea*
[3]*Canadian Institute for Advanced Research, CIFAR Program in Quantum Materials, Toronto, Ontario M5G 1M1, Canada*

(Received 11 September 2023; revised 28 November 2023; accepted 27 February 2024; published 1 April 2024)

Recent experiments on kagome metals AV_3Sb_5 ($A = Cs, Rb, K$) indicated spontaneous time-reversal symmetry breaking in the charge density wave state in the absence of static magnetization. The loop current order (LCO) is proposed as its cause, but a microscopic model explaining the emergence of LCO through electronic correlations has not been firmly established. We show that the coupling between van Hove singularities with distinct mirror symmetries is a key ingredient to generate LCO ground state. By constructing an effective model, we find that when multiple van Hove singularities with opposite mirror eigenvalues are close in energy, the nearest-neighbor electron repulsion favors a ground state with coexisting LCO and charge bond order. It is then demonstrated that this mechanism applies to the kagome metals AV_3Sb_5. Our findings provide an intriguing mechanism of LCO and pave the way for a deeper understanding of complex quantum phenomena in kagome systems.

DOI: 10.1103/PhysRevLett.132.146501

Introduction.—The vanadium-based kagome metals AV_3Sb_5 ($A = Cs, Rb, K$) have generated considerable interest due to the discovery of exotic phases in this family of materials [1–28]. Superconductivity in these materials emerges at $T_c \sim 0.9$–2.8 K [29–32], with magnetoresistance measurements indicating the possibility of novel superconductivity with charge 4e and 6e flux quantization [33]. Additionally, a 2×2 charge density wave (CDW) is detected below $T_{\mathrm{CDW}} \sim 80$–100 K [29,34–38] with scanning tunneling microscopy, emphasizing the important role of van Hove singularities (vHSs) at M point of the Brillouin zone. Intriguingly, these materials exhibit spontaneous time-reversal symmetry breaking after the CDW transition, evidenced through techniques such as muon spin relaxation and scanning tunneling microscope [12,35,39] in the CDW phase without evidence of static magnetic order [30,34,40]. These observations indicate an unconventional CDW order in AV_3Sb_5.

The observation of time-reversal symmetry breaking without static magnetic order leads to the hypothesis of loop current order (LCO) [12,41–43], but the mechanism to generate LCO remains unclear. Enormous experimental and theoretical efforts are devoted to determine the properties of CDW in this kagome system [9,13,20,36,42–72]. The simplest way to model the system is through a three-band model obtained by assigning a single orbital to each site. When the chemical potential is close to the vHS, incorporating nearest neighbor (NN) electron interactions and electron-phonon coupling leads to a charge bond order (CBO) ground state rather than LCO [20]. Reference [43] shows that LCO can be induced by electron interaction, but this necessitates a substantial next-nearest-neighbor interaction, a condition not aligned with realistic scenarios. This poses a critical question: what are the conditions for the emergence of LCO in generic kagome materials?

Noticing the presence of multiple vHSs in AV_3Sb_5, in this Letter we demonstrate that when two vHSs with *different mirror symmetry eigenvalues* are close to the Fermi level, a simple NN interaction can generate LCO when the coupling between different vHSs is taken into account. This ground state has LCO coexisting with CBO, dubbed loop current charge bond order (LCBO). We apply this analysis to AV_3Sb_5 by considering a tight binding model with multiple vHSs. We find that the ground state of AV_3Sb_5 is LCBO under the conditions described below. This study unveils a mechanism for generating LCO in kagome systems with multiple vHSs.

Conditions imposed by mirror symmetries.—We first show that mirror symmetries impose important constraints on the wave functions at vHSs, which are key ingredients for the emergence of LCBO. Each vHS at momentum M has little group D_{2h} with mutually perpendicular mirror planes m_z, m', m'', where m_z coincides with kagome plane, m' and m'' are shown in Fig. 1(a). Consider two vHSs near the Fermi level denoted by VH1 and VH2 at the three distinct momenta M denoted by M_A, M_B, M_C as in Fig. 1(a). We show that mirror symmetries will constrain the wave function of VH1 and VH2 at three distinct M points to take the form of Fig. 1(c) as long as the following conditions are satisfied: (1) the wave functions of VH1 and VH2 have opposite eigenvalues under m' and the same eigenvalues under m'', and (2) VH1 and VH2 consist of the same type of orbital at the kagome sites.

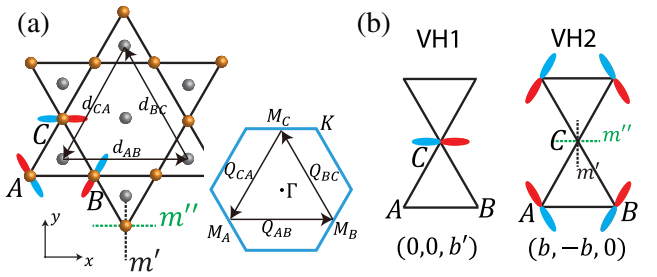

(c)

	M_A	M_B	M_C
VH1	$(b',0,0)$	$(0,b',0)$	$(0,0,b')$
VH2	$(0,b,-b)$	$(-b,0,b)$	$(b,-b,0)$

FIG. 1. (a) Kagome plane of AV_3Sb_5 (A = Cs, Rb, K). The red (blue) parts denote regions of orbitals with positive (negative) amplitude. The inset shows the Brillouin zone. (b) Real space wave function of VH1 and VH2 at M_C allowed by mirror symmetries. (c) Weight of wave function in (A, B, C) sublattices for VH1 and VH2 at three distinct M points imposed by mirror symmetries, where b and b' are constants.

To demonstrate this conclusion explicitly, we consider two vHSs made of the colored orbitals in Fig. 1(a), and let the wave function at VH1 (VH2) be odd (even) under m'. Let us inspect the form of symmetry-allowed wave function at momentum M_c as shown in Fig. 1(b). In this case, m' coincides with m_x, which maps sublattice A and B to each other and maps sublattice C to itself. Because the wave function of VH2 is even under m' and the orbital at sublattice C is odd under m', the weight of wave function must vanish at m'-invariant sublattice C. Furthermore, wave function components of VH2 at sublattice A and B must have opposite signs to make the wave function even under m'. Therefore, the wave function of VH2 at momentum M_C must take the form $(b, -b, 0)$ at A, B, C sublattices respectively, where b is a constant. A similar analysis can be applied to VH1, which gives the form of $(0, 0, b')$ instead, where b' is another constant. Finally, the threefold rotation symmetry leads to the wave function structure at the three distinct M points given in Fig. 1(c). Similarly, this wave function structure can also be obtained for orbitals with other mirror eigenvalues, as shown in Sec. I of the Supplemental Material (SM) [73].

Effective model for coupled vHSs.—We construct an effective model that describes the coupling between different vHSs. The order parameter for a complex CDW with 2×2 periodicity is written as

$$\Delta_{\alpha\beta} = \frac{V}{2N_c}\sum_{\mathbf{R}}\left(\langle c^\dagger_{\mathbf{R},\alpha} c_{\mathbf{R},\beta}\rangle - \langle c^\dagger_{\mathbf{R},\alpha} c_{\mathbf{R}-\mathbf{d}_{\alpha\beta},\beta}\rangle\right)\cos(\mathbf{Q}_{\alpha\beta}\cdot\mathbf{R}). \tag{1}$$

Here, $\mathbf{R}$ labels unit cells, V is the NN interaction strength, N_c is the number of unit cells, $\alpha, \beta = A, B, C$ denote the kagome sublattices, and $\mathbf{Q}_{\alpha\beta}$ connects different momenta M as in Fig. 1(a). In phases that preserve threefold rotation symmetry, the order parameters satisfy $\Delta_{AB} = \Delta_{BC} = \Delta_{CA} \equiv \Delta$. The real part of Δ represents CBO, the imaginary part represents LCO, and a complex value of Δ represents the coexisting phase of LCO and CBO, denoted as LCBO in Fig. 2(a). The phase with real $\Delta > 0$ ($\Delta < 0$) is denoted as CBO^+ (CBO^-) as shown in Figs. 2(b) and 2(c). There are other possible LCO phases distinct from the ones in Fig. 2, but those phases have higher free energy as shown in Sec. IV of SM; hence, we mainly focus on the phases in Fig. 2.

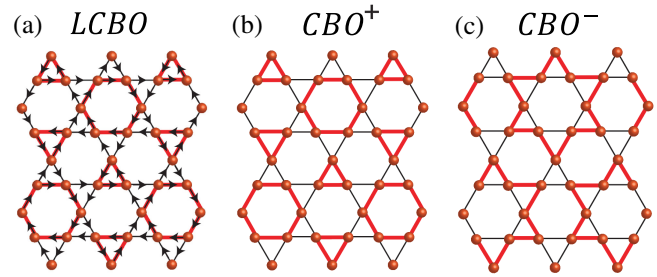

FIG. 2. (a) Coexisting loop current order and charge bond order (LCBO). The red bonds represent modulations of $\langle c^\dagger_{\mathbf{r}} c_{\mathbf{r}'}\rangle$ at NN bonds and the arrows represent current $I \sim \langle i c^\dagger_{\mathbf{r}} c_{\mathbf{r}'} - i c^\dagger_{\mathbf{r}'} c_{\mathbf{r}}\rangle$. (b) Charge bond order with $\Delta > 0$. (c) Charge bond order with $\Delta < 0$.

We can construct an effective model on patches near the three M points. This model can effectively capture the coupling between different vHSs, which is the dominant contribution leading to the LCBO ground state. The coupling between vHSs at different M points is proportional to the order parameter with coupling strength determined by the wave function components at vHSs. We choose the basis $u_1(M_A), u_1(M_B), u_1(M_C), u_2(M_A), u_2(M_B), u_2(M_C)$ where u_1, u_2 denotes the wave function for VH1 and VH2 respectively. Let $\mathbf{k}$ denote the small deviation from M with $|\mathbf{k}| < k_{\mathrm{cut}}$. Given the form of wave functions in Fig. 1(c) and the order parameter in Eq. (1), the effective Hamiltonian with leading terms in $\mathbf{k}$ is derived in Sec. II of SM to be

$$H_{\mathrm{eff}}(\mathbf{k},\Delta) = \begin{pmatrix} \epsilon_1 & s_1\Delta & s_1\Delta^* & \lambda^* k_1 & 0 & 0 \\ s_1\Delta^* & \epsilon_1 & s_1\Delta & 0 & \lambda^* k_2 & 0 \\ s_1\Delta & s_1\Delta^* & \epsilon_1 & 0 & 0 & \lambda^* k_3 \\ \lambda k_1 & 0 & 0 & \epsilon_2 & s_2\Delta^* & s_2\Delta \\ 0 & \lambda k_2 & 0 & s_2\Delta & \epsilon_2 & s_2\Delta^* \\ 0 & 0 & \lambda k_3 & s_2\Delta^* & s_2\Delta & \epsilon_2 \end{pmatrix}, \equiv \begin{pmatrix} P_1 & Q^\dagger \\ Q & P_2 \end{pmatrix}. \tag{2}$$

Here, P_1, P_2, Q are 3×3 matrices, $k_1 = -\frac{1}{2}k_x + (\sqrt{3}/2)k_y$, $k_2 = -\frac{1}{2}k_x - (\sqrt{3}/2)k_y$, $k_3 = k_x$. ϵ_1 and ϵ_2 denote the

energies of VH1 and VH2, respectively. The chemical potential μ is set between ϵ_1 and ϵ_2. Let us first inspect the form of P matrices imposed by symmetries. The matrix P_1 (P_2) describes the effect of CDW order on VH1 (VH2) at momenta M_A, M_B, M_C. The threefold rotation symmetry permutes the three M points, which requires $(P_n)_{12} = (P_n)_{23} = (P_n)_{31}$ for $n = 1, 2$, and whether these matrix elements are related to Δ or Δ^* is determined by the wave function at the vHS. The coefficients s_1 and s_2 are determined by wave functions at the vHS, which are found to be $s_1 = -2|b'|^2$ and $s_2 = 2|b|^2$. The relative sign difference in these coefficients comes from the $-b$ term in Fig. 1(c) as shown in Sec. III of SM, which is a consequence of the mirror symmetries.

Another important consequence of the mirror symmetries is that they enforce the Q matrix in the off-diagonal block to be a diagonal matrix. With the wave function structure in Fig. 1(c), the off-diagonal elements of Q must vanish because they are multiplied by the zeros of wave function components from either VH1 or VH2, as shown in Sec. III of SM. Therefore, only the diagonal terms remain in the Q matrix, which describes the coupling between two vHSs at the same M point. These terms are linear in $\mathbf{k}$ because ϵ_1 and ϵ_2 are exact eigenvalues when both $\mathbf{k}$ and Δ are zero; hence, at $\mathbf{k} = 0$ the diagonal terms should vanish and the leading order is linear in $\mathbf{k}$.

Mechanism to generate LCBO.—We now discuss the last condition for LCBO to be the ground state of a system described by Eq. (2). To derive this, we start from the limit with $\lambda = 0$ and do a perturbation theory on λ. When $\lambda = 0$, $H_{\mathrm{eff}}(\mathbf{k}, \Delta)$, and $H_{\mathrm{eff}}(\mathbf{k}, \Delta e^{(2\pi i/3)})$ have the same eigenvalues because they are related by a gauge transformation $\mathcal{U} = \mathrm{diag}\{1, \omega, \omega^*, 1, \omega^*, \omega\}$ with $\omega = e^{(2\pi i/3)}$. Hence, when $\lambda = 0$ the free energy F is invariant under $\Delta \to \Delta e^{(2\pi/3)i}$, and F has degenerate minima at $\Delta = -|\Delta|$ and $\Delta = |\Delta| e^{\pm(\pi/3)i}$ corresponding to CBO$^-$ and LCBO respectively. The eigenvalues of $H_{\mathrm{eff}} - \mu$ at both minima are the same, which are given by

$$E_1 = \epsilon_2 - \mu - 4|b|^2|\Delta|, \quad E_2 = E_3 = \epsilon_1 - \mu - 2|b'|^2|\Delta|,$$
$$E_4 = E_5 = \epsilon_2 - \mu + 2|b|^2|\Delta|, \quad E_6 = \epsilon_1 - \mu + 4|b'|^2|\Delta|. \tag{3}$$

When the energy separation between VH1 and VH2 is small, the sign of each eigenvalue is determined by the Δ term; hence, the negative eigenvalues are E_1, E_2, E_3. In the low-temperature limit the sum of them determines the free energy. When λ becomes finite, the degenerate minima of F at $\Delta = -|\Delta|$ and $|\Delta| e^{\pm(\pi/3)i}$, corresponding to CBO$^-$ and LCBO splits. The amount of splitting can be computed by degenerate perturbation theory that captures the evolution of $E_{1\text{–}3}$ with λ. Define $\delta\epsilon \equiv \epsilon_2 - \epsilon_1$ as the separation between VH1 and VH2 and denote A as the system area. We find that the difference in free energy density $f = F/A$ between CBO$^-$ and LCBO is given by

$$\begin{aligned} f_{\mathrm{CBO}^-} - f_{\mathrm{LCBO}} &= \sum_{|\mathbf{k}| \lesssim k_{\mathrm{cut}}} \frac{-2|\lambda|^2 (k_1 k_2 + k_2 k_3 + k_1 k_3)|\Delta|(|b|^2 + |b'|^2)}{A(2|\Delta|(|b|^2 + |b'|^2) + \delta\epsilon)(4|\Delta|(|b|^2 + |b'|^2) - \delta\epsilon)} \\ &= \frac{3}{16\pi} \frac{|\lambda|^2 k_{\mathrm{cut}}^4 |\Delta|(|b|^2 + |b'|^2)}{(2|\Delta|(|b|^2 + |b'|^2) + \delta\epsilon)(4|\Delta|(|b|^2 + |b'|^2) - \delta\epsilon)} > 0. \end{aligned} \tag{4}$$

Equation (4) shows that for small energy separation $\delta\epsilon < 4(|b|^2 + |b'|^2)|\Delta|$, a finite coupling λ between the two vHSs will make LCBO have lower energy and be more favorable than the competing phase CBO$^-$. This is the mechanism to generate LCBO in kagome systems.

Importantly, we find that the LCBO phase cannot be described by a small order parameter expansion of the Ginzburg-Landau theory; hence, it is not sensitive to the dispersion near vHSs. In Sec. V of SM, we demonstrate that the solution corresponding to LCBO cannot be obtained from Ginzburg-Landau free energy even if high power terms of Δ are included. We also reiterate that the free energy analysis in Eq. (4) leading to an LCBO ground state is a result of the coupling between two vHSs with distinct mirror symmetries.

Application to AV_3Sb_5.—We apply the above analysis to AV_3Sb_5 and explicitly construct the effective Hamiltonian H_{eff}. We start from a tight binding model that captures multiple vHSs near the Fermi level. The bands close to the Fermi level in AV_3Sb_5 are mainly made of d orbitals at V sites and p orbitals at Sb sites. We consider the tight binding model introduced in Ref. [68]. This model includes three p orbitals at each out-of-plane Sb site and one d orbital at each V site. This d orbital is made of a specific linear combination of d_{xz}, d_{yz} orbitals as indicated by the colored orbitals in Fig. 1(a), which is odd (even) under m' (m''), denoted as $\tilde{d}$ orbitals. Hence, there are three $\tilde{d}$ orbitals and six p orbitals in each unit cell, leading to a nine-band model $H_{\mathrm{TB}}(\mathbf{k})$. The hopping parameters in this model are obtained from density-functional theory (DFT) band structure [68]. The band structure of $H_{\mathrm{TB}}(\mathbf{k})$ is shown in Fig. 3(a). Compared with the DFT band structure in Fig. 3(b), the nine-band model reproduces two vHSs at momentum M denoted by VH1 and VH2. VH1 is odd (even) under m' (m'') and is mainly made of $\tilde{d}$ orbitals. VH2 is even under both m' and m'' and is a superposition of $\tilde{d}$ and p orbitals. Compared with commonly used three-band models that can only describe VH1, this nine-band model can capture both VH1 and VH2; hence, it provides a useful platform to study the interplay between different vHSs.

Next we consider the NN electron interaction given by

$$H_V = V \sum_{\langle \mathbf{R}\alpha; \mathbf{R}'\beta \rangle} c^\dagger_{\mathbf{R},\alpha} c_{\mathbf{R},\alpha} c^\dagger_{\mathbf{R}',\beta} c_{\mathbf{R}',\beta}, \tag{5}$$

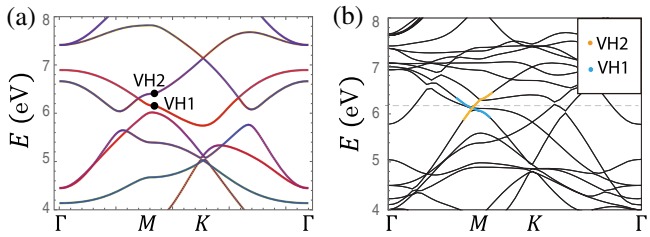

FIG. 3. (a) Band structure of the 9×9 tight binding model $H_{\mathrm{TB}}(\mathbf{k})$ that can reproduce VH1 and VH2. The red color represents the weight of $\tilde{d}$ orbitals in the wave function. (b) Band structure obtained from DFT with VH1 and VH2 highlighted. The figure is adapted from Ref. [68].

where $\langle \mathbf{R}\alpha; \mathbf{R}'\beta \rangle$ denotes NN bonds. With the order parameter $\Delta_{\alpha\beta}$ defined in Eq. (1), the NN interaction can be mean-field decoupled as [68]

$$H_V^{\mathrm{MF}} = -\sum_{\mathbf{k}} \left(\Delta_{\alpha\beta} (1 - e^{i\mathbf{k}\cdot\mathbf{d}_{\alpha\beta}}) c^{\dagger}_{\mathbf{k}-\mathbf{Q}_{\alpha\beta},\beta} c_{\mathbf{k},\alpha} + \mathrm{H.c.} \right) + 2N_c \frac{|\Delta_{\alpha\beta}|^2}{V}, \tag{6}$$

We can write down a mean-field Hamiltonian that includes all bands in Fig. 3(a) and the CDW order parameter in Eq. (6) with $\Delta_{AB} = \Delta_{BC} = \Delta_{CA} \equiv \Delta$. To construct the effective patch model H_{eff}, we focus on momenta near the M points and perform a unitary transformation into the band basis in which the basis functions at M points are eigenfunctions of the tight binding model. Then we keep only the matrix elements corresponding to the energies and couplings between VH1 and VH2. This leads to a 6×6 matrix $H_{\mathrm{eff}}(\mathbf{k}, \Delta)$ corresponding to the six patches at VH1 and VH2 near the three M points. By performing a Taylor expansion in $\mathbf{k}$ and keeping leading order terms, we obtain H_{eff} in Eq. (2) with parameters $\epsilon_1 = 6.16$ eV, $\epsilon_2 = 6.40$ eV, $b = 0.52$, $b' = 0.96$, $\lambda = 0.35$ eV a, where $a = 5.48$ Å is the lattice constant. Because the wave functions at both vHSs have significant weight on $\tilde{d}$ orbitals, the coupling λ between the two vHSs receives major contribution from the hopping amplitude t_{dd} between nearest-neighbor $\tilde{d}$ orbitals; hence, λ is generally nonzero. With a finite λ, the above theory for LCBO is applicable to AV_3Sb_5, indicating that the LCBO phase can be stabilized as the ground state.

Phase diagram of CDW orders.—The phase diagram of H_{eff} obtained by minimizing the free energy with respect to Δ at different chemical potential and interaction strength is shown in Fig. 4(a). The LCBO phase is more pronounced near VH2 due to the difference in wave function structures at VH1 and VH2. Equation (4) requires the eigenvalues $E_{1\text{–}3}$ be negative and $E_{4\text{–}6}$ be positive. Based on Eq. (3), these conditions lead to $4|b'|^2|\Delta| > \delta\epsilon$ when $\mu \sim \epsilon_2$, while when $\mu \sim \epsilon_1$ they lead to $4|b|^2|\Delta| > \delta\epsilon$. Since $|b'| > |b|$ due to the larger weight of $\tilde{d}$ orbital at VH1, when $\mu \sim \epsilon_2$ it requires smaller $|\Delta|$ and smaller interaction to realize LCBO. This leads to the smaller critical interaction strength near VH2 as shown in the phase diagram. The competition between CBO^- and LCBO depends on the strength of λ. The free energy of the CBO^- and LCBO phases at $\mu = \epsilon_2$, $V = 1.3$ eV as a function of coupling strength λ is shown in Fig. 4(b). It shows LCBO and CBO^- are degenerate when $\lambda = 0$, and a finite λ makes the free energy of LCBO lower than CBO^-, consistent with Eq. (4).

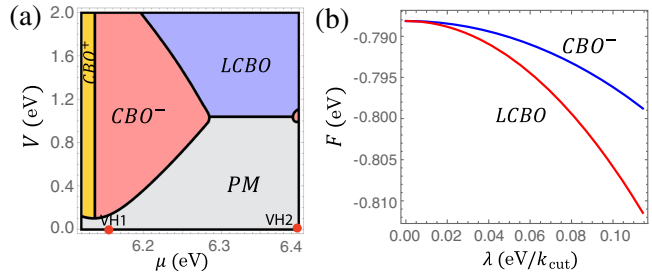

FIG. 4. (a) Phase diagram of H_{eff} at different interaction strengths and chemical potential with parameters $\epsilon_1 = 6.16$ eV, $\epsilon_2 = 6.40$ eV, $b = 0.52$, $b' = 0.96$, $\lambda k_{\mathrm{cut}} = 0.1$ eV and temperature is 90 K. *PM* refers to the pristine metal without any CDW order. (b) Free energy of LCBO and CBO^- as a function of coupling λ at a fixed interaction strength. It shows LCBO is favored at finite λ.

Effects of the other bands.—In AV_3Sb_5 there are other bands near the Fermi level and their effects need to be investigated. For this purpose, we consider an effective patch model obtained by adding one more band below VH1 (denoted as ϵ_3) in Fig. 3(a) to H_{eff}, which expands it to a 9×9 matrix near the M points. This model includes VH1, VH2, and ϵ_3, and its phase diagram is shown in Fig. 5(a). Compared with Fig. 4(a), which only includes VH1 and VH2, the key variation in Fig. 5(a) occurs near VH1, which is close to the additional band at ϵ_3. However, in regions around VH2 that are more distant from ϵ_3, the two phase diagrams resemble each other, with LCBO emerging in

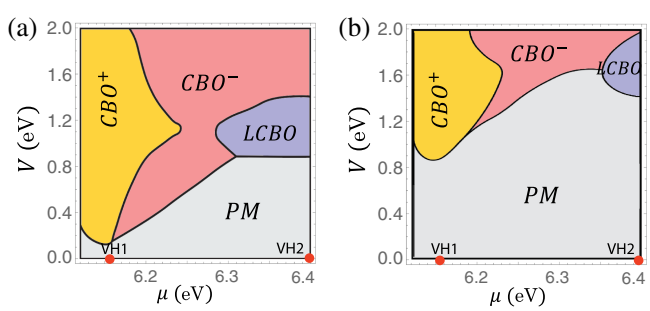

FIG. 5. (a) Phase diagram of the effective patch model obtained by including VH1, VH2, and ϵ_3. *PM* refers to the pristine metal without any CDW order. (b) Phase diagram that takes into account all bands in H_{TB} and the momentum summation is over the Brillouin zone. The LCBO phase still exists near VH2.

both scenarios. We further demonstrate that the emergence of LCBO inferred from the patch model remains valid when all the bands in the tight binding model are considered and the momentum cutoff is removed. The phase diagram obtained with all bands in $H_{\mathrm{TB}}(\mathbf{k})$ included is shown in Fig. 5(b). The real space configuration of these phases are shown in Fig. 2 with the order parameter given in Eq. (1). The summation of momentum in computing the free energy is taken over the whole Brillouin zone. The LCBO phase exists near VH2, whereas near VH1 the ground state is CBO, due to the effect of band structure away from M points and the other bands that are not taken into account in the patch models. This comparison suggests despite the quantitative difference in these phase diagrams, our main finding of LCBO remains valid in the full-band model as long as the chemical potential is near VH2.

Discussion.—We provide a mechanism to realize LCBO in kagome systems based on the coupling between multiple vHSs with different mirror symmetries. The imaginary part of LCBO breaks time-reversal symmetry, whereas the real part of LCBO can induce lattice distortion with star of David or trihexagonal patterns. Experiments on AV_3Sb_5 have observed staggered patterns of lattice distortion among different kagome layers [26]. If the ground state is described by LCBO, we expect the loop current order to be staggered along the c axis as well. Our theory shows LCBO is more favorable when the energy difference $\delta\epsilon$ between vHSs is small. Experiments and first-principle computations suggest that pressure can lead to an increase of $\delta\epsilon$ [45,72]; hence, we expect LCBO to disappear under high pressure, which is consistent with the disappearance of CDW under high pressure observed in experiments [31,48,65,70]. The phase diagram of AV_3Sb_5 in Fig. 5(b) suggests that LCBO emerges when the chemical potential is close to VH2. Thus we predict that electron doping the material is more likely to induce the LCBO phase. Given the general applicability of our theory to kagome systems having vHSs with distinct mirror eigenvalues, we hope this work will inspire further exploration of kagome materials with mirror symmetries.

This work is supported by the Natural Sciences and Engineering Research Council of Canada (NSERC) Discovery Grant No. 2022-04601, No. RGPIN-2023-03296 and the Center for Quantum Materials at the University of Toronto. H. Y. K. acknowledges the support of the Canadian Institute for Advanced Research (CIFAR) and the Canada Research Chairs Program. Y. B. K. is supported by the Simons Fellowship from the Simons Foundation and the Guggenheim Fellowship from the John Simon Guggenheim Memorial Foundation. Computations were performed on the Niagara supercomputer at the SciNet HPC Consortium. SciNet is funded by: the Canada Foundation for Innovation under the auspices of Compute Canada; the Government of Ontario; Ontario Research Fund—Research Excellence; and the University of Toronto.

*ybkim@physics.utoronto.ca
†hykee@physics.utoronto.ca

[1] Kun Jiang, Tao Wu, Jia-Xin Yin, Zhenyu Wang, M. Zahid Hasan, Stephen D. Wilson, Xianhui Chen, and Jiangping Hu, Kagome superconductors AV_3Sb_5 ($A = K, Rb, Cs$), Natl. Sci. Rev. **10**, nwac199 (2022).

[2] Shuo-Ying Yang, Yaojia Wang, Brenden R. Ortiz, Defa Liu, Jacob Gayles, Elena Derunova, Rafael Gonzalez-Hernandez, Libor Šmejkal, Yulin Chen, Stuart S. P. Parkin, Stephen D. Wilson, Eric S. Toberer, Tyrel McQueen, and Mazhar N. Ali, Giant, unconventional anomalous Hall effect in the metallic frustrated magnet candidate, KV_3Sb_5, Sci. Adv. **6**, eabb6003 (2020).

[3] Titus Neupert, M. Michael Denner, Jia-Xin Yin, Ronny Thomale, and M. Zahid Hasan, Charge order and superconductivity in kagome materials, Nat. Phys. **18**, 137 (2022).

[4] Yaojia Wang, Shuoying Yang, Pranava K. Sivakumar, Brenden R. Ortiz, Samuel M. L. Teicher, Heng Wu, Abhay K. Srivastava, Chirag Garg, Defa Liu, Stuart S. P. Parkin, Eric S. Toberer, Tyrel McQueen, Stephen D. Wilson, and Mazhar N. Ali, Proximity-induced spin-triplet superconductivity and edge supercurrent in the topological kagome metal, $K_{1-x}V_3Sb_5$, arXiv:2012.05898.

[5] Yong Hu, Xianxin Wu, Brenden R. Ortiz, Sailong Ju, Xinloong Han, Junzhang Ma, Nicholas C. Plumb, Milan Radovic, Ronny Thomale, Stephen D. Wilson, Andreas P. Schnyder, and Ming Shi, Rich nature of Van Hove singularities in kagome superconductor CsV_3Sb_5, Nat. Commun. **13**, 2220 (2022).

[6] Yuzki M. Oey, Brenden R. Ortiz, Farnaz Kaboudvand, Jonathan Frassineti, Erick Garcia, Rong Cong, Samuele Sanna, Vesna F. Mitrović, Ram Seshadri, and Stephen D. Wilson, Fermi level tuning and double-dome superconductivity in the kagome metal $CsV_3Sb_{5-x}Sn_x$, Phys. Rev. Mater. **6**, L041801 (2022).

[7] Morten H. Christensen, Turan Birol, Brian M. Andersen, and Rafael M. Fernandes, Loop currents in AV_3Sb_5 kagome metals: Multipolar and toroidal magnetic orders, Phys. Rev. B **106**, 144504 (2022).

[8] C. C. Zhu, X. F. Yang, W. Xia, Q. W. Yin, L. S. Wang, C. C. Zhao, D. Z. Dai, C. P. Tu, B. Q. Song, Z. C. Tao, Z. J. Tu, C. S. Gong, H. C. Lei, Y. F. Guo, and S. Y. Li, Double-dome superconductivity under pressure in the v-based kagome metals AV_3Sb_5 (a = Rb and k), Phys. Rev. B **105**, 094507 (2022).

[9] Q. Stahl, D. Chen, T. Ritschel, C. Shekhar, E. Sadrollahi, M. C. Rahn, O. Ivashko, M. v. Zimmermann, C. Felser, and J. Geck, Temperature-driven reorganization of electronic order in CsV_3Sb_5, Phys. Rev. B **105**, 195136 (2022).

[10] Shangfei Wu, Brenden R. Ortiz, Hengxin Tan, Stephen D. Wilson, Binghai Yan, Turan Birol, and Girsh Blumberg, Charge density wave order in the kagome metal AV_3Sb_5 ($a = Cs, Rb, K$), Phys. Rev. B **105**, 155106 (2022).

[11] Mingu Kang, Shiang Fang, Jeong-Kyu Kim, Brenden R. Ortiz, Sae Hee Ryu, Jimin Kim, Jonggyu Yoo, Giorgio Sangiovanni, Domenico Di Sante, Byeong-Gyu Park, Chris Jozwiak, Aaron Bostwick, Eli Rotenberg, Efthimios Kaxiras, Stephen D. Wilson, Jae-Hoon Park, and Riccardo Comin, Twofold Van Hove singularity and origin

of charge order in topological kagome superconductor CsV_3Sb_5, Nat. Phys. **18**, 301 (2022).

[12] Yu-Xiao Jiang *et al.*, Unconventional chiral charge order in kagome superconductor Kv_3Sb_5, Nat. Mater. **20**, 1353 (2021).

[13] Haoxiang Li, T. T. Zhang, T. Yilmaz, Y. Y. Pai, C. E. Marvinney, A. Said, Q. W. Yin, C. S. Gong, Z. J. Tu, E. Vescovo, C. S. Nelson, R. G. Moore, S. Murakami, H. C. Lei, H. N. Lee, B. J. Lawrie, and H. Miao, Observation of unconventional charge density wave without acoustic phonon anomaly in kagome superconductors AV_3Sb_5 ($a = \mathrm{Rb}$, Cs), Phys. Rev. X **11**, 031050 (2021).

[14] Xianxin Wu, Tilman Schwemmer, Tobias Müller, Armando Consiglio, Giorgio Sangiovanni, Domenico Di Sante, Yasir Iqbal, Werner Hanke, Andreas P. Schnyder, M. Michael Denner, Mark H. Fischer, Titus Neupert, and Ronny Thomale, Nature of unconventional pairing in the kagome superconductors AV_3Sb_5 ($a = \mathrm{K}, \mathrm{Rb}, \mathrm{Cs}$), Phys. Rev. Lett. **127**, 177001 (2021).

[15] He Zhao, Hong Li, Brenden R. Ortiz, Samuel M. L. Teicher, Takamori Park, Mengxing Ye, Ziqiang Wang, Leon Balents, Stephen D. Wilson, and Ilija Zeljkovic, Cascade of correlated electron states in the kagome superconductor CsV_3Sb_5, Nature (London) **599**, 216 (2021).

[16] Hong Li, He Zhao, Brenden R. Ortiz, Takamori Park, Mengxing Ye, Leon Balents, Ziqiang Wang, Stephen D. Wilson, and Ilija Zeljkovic, Rotation symmetry breaking in the normal state of a kagome superconductor KV_3Sb_5, Nat. Phys. **18**, 265 (2022).

[17] Astrid T. Rømer, Shinibali Bhattacharyya, Roser Valentí, Morten H. Christensen, and Brian M. Andersen, Superconductivity from repulsive interactions on the kagome lattice, Phys. Rev. B **106**, 174514 (2022).

[18] Thomas Mertz, Paul Wunderlich, Shinibali Bhattacharyya, Francesco Ferrari, and Roser Valentí, Statistical learning of engineered topological phases in the kagome superlattice of AV_3Sb_5, npj Comput. Mater. **8**, 66 (2022).

[19] Andrzej Ptok, Aksel Kobiałka, Małgorzata Sternik, Jan Łażewski, Paweł T. Jochym, Andrzej M. Oleś, and Przemysław Piekarz, Dynamical study of the origin of the charge density wave in AV_3Sb_5 ($a = \mathrm{K}$, Rb, Cs) compounds, Phys. Rev. B **105**, 235134 (2022).

[20] Francesco Ferrari, Federico Becca, and Roser Valentí, Charge density waves in kagome-lattice extended Hubbard models at the Van Hove filling, Phys. Rev. B **106**, L081107 (2022).

[21] Ece Uykur, Brenden R. Ortiz, Stephen D. Wilson, Martin Dressel, and Alexander A. Tsirlin, Optical detection of the density-wave instability in the kagome metal KV_3Sb_5, npj Quantum Mater. **7**, 16 (2022).

[22] Francesco Grandi, Armando Consiglio, Michael A. Sentef, Ronny Thomale, and Dante M. Kennes, Theory of nematic charge orders in kagome metals, Phys. Rev. B **107**, 155131 (2023).

[23] Yishuai Xu, Zhuoliang Ni, Yizhou Liu, Brenden R. Ortiz, Qinwen Deng, Stephen D. Wilson, Binghai Yan, Leon Balents, and Liang Wu, Three-state nematicity and magneto-optical Kerr effect in the charge density waves in kagome superconductors, Nat. Phys. **18**, 1470 (2022).

[24] David R. Saykin, Camron Farhang, Erik D. Kountz, Dong Chen, Brenden R. Ortiz, Chandra Shekhar, Claudia Felser, Stephen D. Wilson, Ronny Thomale, Jing Xia, and Aharon Kapitulnik, High resolution polar Kerr effect studies of CsV_3Sb_5: Tests for time-reversal symmetry breaking below the charge-order transition, Phys. Rev. Lett. **131**, 016901 (2023).

[25] Yajian Hu, Soichiro Yamane, Giordano Mattoni, Kanae Yada, Keito Obata, Yongkai Li, Yugui Yao, Zhiwei Wang, Jingyuan Wang, Camron Farhang, Jing Xia, Yoshiteru Maeno, and Shingo Yonezawa, Time-reversal symmetry breaking in charge density wave of CsV_3Sb_5 detected by polar Kerr effect, arXiv:2208.08036.

[26] Mingu Kang, Shiang Fang, Jonggyu Yoo, Brenden R. Ortiz, Yuzki M. Oey, Jonghyeok Choi, Sae Hee Ryu, Jimin Kim, Chris Jozwiak, Aaron Bostwick, Eli Rotenberg, Efthimios Kaxiras, Joseph G. Checkelsky, Stephen D. Wilson, Jae-Hoon Park, and Riccardo Comin, Charge order landscape and competition with superconductivity in kagome metals, Nat. Mater. **22**, 186 (2022).

[27] Jingyuan Wang, Camron Farhang, Brenden R. Ortiz, Stephen D. Wilson, and Jing Xia, Resolving the discrepancy between MOKE measurements at 1550-nm wavelength on kagome metal CsV_3Sb_5, Phys. Rev. Mater. **8**, 014202 (2024).

[28] Stephen D. Wilson and Brenden R. Ortiz, AV_3Sb_5 kagome superconductors: Progress and future directions, arXiv:2311.05946.

[29] Brenden R. Ortiz, Samuel M. L. Teicher, Yong Hu, Julia L. Zuo, Paul M. Sarte, Emily C. Schueller, A. M. Milinda Abeykoon, Matthew J. Krogstad, Stephan Rosenkranz, Raymond Osborn, Ram Seshadri, Leon Balents, Junfeng He, and Stephen D. Wilson, CsV_3Sb_5: A $\mathbb{Z}_2$ topological kagome metal with a superconducting ground state, Phys. Rev. Lett. **125**, 247002 (2020).

[30] Brenden R. Ortiz, Paul M. Sarte, Eric M. Kenney, Michael J. Graf, Samuel M. L. Teicher, Ram Seshadri, and Stephen D. Wilson, Superconductivity in the $\mathbb{Z}_2$ kagome metal KV_3Sb_5, Phys. Rev. Mater. **5**, 034801 (2021).

[31] K. Y. Chen, N. N. Wang, Q. W. Yin, Y. H. Gu, K. Jiang, Z. J. Tu, C. S. Gong, Y. Uwatoko, J. P. Sun, H. C. Lei, J. P. Hu, and J.-G. Cheng, Double superconducting dome and triple enhancement of T_c in the kagome superconductor CsV_3Sb_5 under high pressure, Phys. Rev. Lett. **126**, 247001 (2021).

[32] Hui Chen *et al.*, Roton pair density wave in a strong-coupling kagome superconductor, Nature (London) **599**, 222 (2021).

[33] Jun Ge, Pinyuan Wang, Ying Xing, Qiangwei Yin, Hechang Lei, Ziqiang Wang, and Jian Wang, Discovery of charge-4e and charge-6e superconductivity in kagome superconductor CsV_3Sb_5,arXiv:2201.10352.

[34] Brenden R. Ortiz, Lídia C. Gomes, Jennifer R. Morey, Michal Winiarski, Mitchell Bordelon, John S. Mangum, Iain W. H. Oswald, Jose A. Rodriguez-Rivera, James R. Neilson, Stephen D. Wilson, Elif Ertekin, Tyrel M. McQueen, and Eric S. Toberer, New kagome prototype materials: Discovery of KV_3Sb_5, RbV_3Sb_5, and CsV_3Sb_5, Phys. Rev. Mater. **3**, 094407 (2019).

[35] Nana Shumiya, Md. Shafayat Hossain, Jia-Xin Yin, Yu-Xiao Jiang, Brenden R. Ortiz, Hongxiong Liu, Youguo Shi, Qiangwei Yin, Hechang Lei, Songtian S. Zhang, Guoqing Chang, Qi Zhang, Tyler A. Cochran, Daniel Multer, Maksim

Litskevich, Zi-Jia Cheng, Xian P. Yang, Zurab Guguchia, Stephen D. Wilson, and M. Zahid Hasan, Intrinsic nature of chiral charge order in the kagome superconductor RbV_3Sb_5, Phys. Rev. B **104**, 035131 (2021).

[36] Brenden R. Ortiz, Samuel M. L. Teicher, Linus Kautzsch, Paul M. Sarte, Noah Ratcliff, John Harter, Jacob P. C. Ruff, Ram Seshadri, and Stephen D. Wilson, Fermi surface mapping and the nature of charge-density-wave order in the kagome superconductor CsV_3Sb_5, Phys. Rev. X **11**, 041030 (2021).

[37] Jian-Guo Si, Wen-Jian Lu, Yu-Ping Sun, Peng-Fei Liu, and Bao-Tian Wang, Charge density wave and pressure-dependent superconductivity in the kagome metal CsV_3Sb_5: A first-principles study, Phys. Rev. B **105**, 024517 (2022).

[38] DianWu Song, LiXuan Zheng, FangHang Yu, Jian Li, LinPeng Nie, Min Shan, Dan Zhao, ShunJiao Li, BaoLei Kang, ZhiMian Wu, YanBing Zhou, KuangLv Sun, Kai Liu, XiGang Luo, ZhenYu Wang, JianJun Ying, XianGang Wan, Tao Wu, and XianHui Chen, Orbital ordering and fluctuations in a kagome superconductor CsV_3Sb_5, Sci. China Phys. Mech. Astron. **65**, 247462 (2022).

[39] C. Mielke, D. Das, J.-X. Yin, H. Liu, R. Gupta, Y.-X. Jiang, M. Medarde, X. Wu, H. C. Lei, J. Chang, Pengcheng Dai, Q. Si, H. Miao, R. Thomale, T. Neupert, Y. Shi, R. Khasanov, M. Z. Hasan, H. Luetkens, and Z. Guguchia, Time-reversal symmetry-breaking charge order in a kagome superconductor, Nature (London) **602**, 245 (2022).

[40] Eric M. Kenney, Brenden R. Ortiz, Chennan Wang, Stephen D. Wilson, and Michael J. Graf, Absence of local moments in the kagome metal KV_3Sb_5 as determined by muon spin spectroscopy, J. Phys. Condens. Matter **33**, 235801 (2021).

[41] Yu-Ping Lin and Rahul M. Nandkishore, Chiral twist on the high-T_c phase diagram in moiré heterostructures, Phys. Rev. B **100**, 085136 (2019).

[42] Hyeok-Jun Yang, Hee Seung Kim, Min Yong Jeong, Yong Baek Kim, Myung Joon Han, and SungBin Lee, Intertwining orbital current order and superconductivity in kagome metal, arXiv:2203.07365.

[43] Jin-Wei Dong, Ziqiang Wang, and Sen Zhou, Loop-current charge density wave driven by long-range coulomb repulsion on the kagomé lattice, Phys. Rev. B **107**, 045127 (2023).

[44] Linpeng Nie *et al.*, Charge-density-wave-driven electronic nematicity in a kagome superconductor, Nature (London) **604**, 59 (2022).

[45] Harrison LaBollita and Antia S. Botana, Tuning the Van Hove singularities in AV_3Sb_5 $(a = \mathrm{K}, \mathrm{Rb}, \mathrm{Cs})$ via pressure and doping, Phys. Rev. B **104**, 205129 (2021).

[46] Hengxin Tan, Yizhou Liu, Ziqiang Wang, and Binghai Yan, Charge density waves and electronic properties of superconducting kagome metals, Phys. Rev. Lett. **127**, 046401 (2021).

[47] Zuowei Liang, Xingyuan Hou, Fan Zhang, Wanru Ma, Ping Wu, Zongyuan Zhang, Fanghang Yu, J.-J. Ying, Kun Jiang, Lei Shan, Zhenyu Wang, and X.-H. Chen, Three-dimensional charge density wave and surface-dependent vortex-core states in a kagome superconductor CsV_3Sb_5, Phys. Rev. X **11**, 031026 (2021).

[48] F. H. Yu, D. H. Ma, W. Z. Zhuo, S. Q. Liu, X. K. Wen, B. Lei, J. J. Ying, and X. H. Chen, Unusual competition of superconductivity and charge-density-wave state in a compressed topological kagome metal, Nat. Commun. **12**, 3645 (2021).

[49] Zhicheng Jiang, Haiyang Ma, Wei Xia, Zhengtai Liu, Qian Xiao, Zhonghao Liu, Yichen Yang, Jianyang Ding, Zhe Huang, Jiayu Liu, Yuxi Qiao, Jishan Liu, Yingying Peng, Soohyun Cho, Yanfeng Guo, Jianpeng Liu, and Dawei Shen, Observation of electronic nematicity driven by the three-dimensional charge density wave in kagome lattice KV_3Sb_5, Nano Lett. **23**, 5625 (2023).

[50] Ethan T. Ritz, Rafael M. Fernandes, and Turan Birol, Impact of sb degrees of freedom on the charge density wave phase diagram of the kagome metal CsV_3Sb_5, Phys. Rev. B **107**, 205131 (2023).

[51] Yong Hu, Xianxin Wu, Brenden R. Ortiz, Xinloong Han, Nicholas C. Plumb, Stephen D. Wilson, Andreas P. Schnyder, and Ming Shi, Coexistence of trihexagonal and star-of-david pattern in the charge density wave of the kagome superconductor AV_3Sb_5, Phys. Rev. B **106**, L241106 (2022).

[52] J. Luo, Z. Zhao, Y. Z. Zhou, J. Yang, A. F. Fang, H. T. Yang, H. J. Gao, R. Zhou, and Guo-qing Zheng, Possible star-of-david pattern charge density wave with additional modulation in the kagome superconductor CsV_3Sb_5, npj Quantum Mater. **7**, 30 (2022).

[53] Chao Mu, Qiangwei Yin, Zhijun Tu, Chunsheng Gong, Ping Zheng, Hechang Lei, Zheng Li, and Jianlin Luo, Tri-hexagonal charge order in kagome metal CsV_3Sb_5 revealed by ^{121}Sb nuclear quadrupole resonance, Chin. Phys. B **31**, 017105 (2022).

[54] Hailan Luo, Qiang Gao, Hongxiong Liu, Yuhao Gu, Dingsong Wu, Changjiang Yi, Junjie Jia, Shilong Wu, Xiangyu Luo, Yu Xu, Lin Zhao, Qingyan Wang, Hanqing Mao, Guodong Liu, Zhihai Zhu, Youguo Shi, Kun Jiang, Jiangping Hu, Zuyan Xu, and X. J. Zhou, Electronic nature of charge density wave and electron-phonon coupling in kagome superconductor KV_3Sb_5, Nat. Commun. **13**, 273 (2022).

[55] Takemi Kato, Yongkai Li, Tappei Kawakami, Min Liu, Kosuke Nakayama, Zhiwei Wang, Ayumi Moriya, Kiyohisa Tanaka, Takashi Takahashi, Yugui Yao, and Takafumi Sato, Three-dimensional energy gap and origin of charge-density wave in kagome superconductor KV_3Sb_5, Commun. Mater. **3**, 30 (2022).

[56] Soohyun Cho, Haiyang Ma, Wei Xia, Yichen Yang, Zhengtai Liu, Zhe Huang, Zhicheng Jiang, Xiangle Lu, Jishan Liu, Zhonghao Liu, Jun Li, Jinghui Wang, Yi Liu, Jinfeng Jia, Yanfeng Guo, Jianpeng Liu, and Dawei Shen, Emergence of new Van Hove singularities in the charge density wave state of a topological kagome metal RbV_3Sb_5, Phys. Rev. Lett. **127**, 236401 (2021).

[57] M. Michael Denner, Ronny Thomale, and Titus Neupert, Analysis of charge order in the kagome metal AV_3Sb_5 $(a = \mathrm{K}, \mathrm{Rb}, \mathrm{Cs})$, Phys. Rev. Lett. **127**, 217601 (2021).

[58] Takamori Park, Mengxing Ye, and Leon Balents, Electronic instabilities of kagome metals: Saddle points and Landau theory, Phys. Rev. B **104**, 035142 (2021).

[59] Yu-Ping Lin and Rahul M. Nandkishore, Complex charge density waves at Van Hove singularity on hexagonal lattices: Haldane-model phase diagram and potential realization in

the kagome metals AV_3Sb_5 ($a = k$, Rb, Cs), Phys. Rev. B **104**, 045122 (2021).

[60] Morten H. Christensen, Turan Birol, Brian M. Andersen, and Rafael M. Fernandes, Theory of the charge density wave in AV_3Sb_5 kagome metals, Phys. Rev. B **104**, 214513 (2021).

[61] Min Yong Jeong, Hyeok-Jun Yang, Hee Seung Kim, Yong Baek Kim, SungBin Lee, and Myung Joon Han, Crucial role of out-of-plane sb p orbitals in Van Hove singularity formation and electronic correlations in the superconducting kagome metal CsV_3Sb_5, Phys. Rev. B **105**, 235145 (2022).

[62] Rina Tazai, Youichi Yamakawa, Seiichiro Onari, and Hiroshi Kontani, Mechanism of exotic density-wave and beyond-migdal unconventional superconductivity in kagome metal AV_3Sb_5 ($a =$ k, Rb, Cs), Sci. Adv. **8**, eabl4108 (2022).

[63] Sen Zhou and Ziqiang Wang, Chern fermi pocket, topological pair density wave, and charge-4e and charge-6e superconductivity in kagomé superconductors, Nat. Commun. **13**, 7288 (2022).

[64] Yi-Ming Wu, Ronny Thomale, and S. Raghu, Sublattice interference promotes pair density wave order in kagome metals, Phys. Rev. B **108**, L081117 (2023).

[65] Haoxiang Li, G. Fabbris, A. H. Said, J. P. Sun, Yu-Xiao Jiang, J.-X. Yin, Yun-Yi Pai, Sangmoon Yoon, Andrew R. Lupini, C. S. Nelson, Q. W. Yin, C. S. Gong, Z. J. Tu, H. C. Lei, J.-G. Cheng, M. Z. Hasan, Ziqiang Wang, Binghai Yan, R. Thomale, H. N. Lee, and H. Miao, Discovery of conjoined charge density waves in the kagome superconductor CsV_3Sb_5, Nat. Commun. **13**, 6348 (2022).

[66] Alexander A. Tsirlin, Pierre Fertey, Brenden R. Ortiz, Berina Klis, Valentino Merkl, Martin Dressel, Stephen D. Wilson, and Ece Uykur, Role of Sb in the superconducting kagome metal CsV_3Sb_5 revealed by its anisotropic compression, SciPost Phys. **12**, 049 (2022).

[67] Jonathan Frassineti, Pietro Bonfà, Giuseppe Allodi, Erick Garcia, Rong Cong, Brenden R. Ortiz, Stephen D. Wilson, Roberto De Renzi, Vesna F. Mitrović, and Samuele Sanna, Microscopic nature of the charge-density wave in the kagome superconductor RbV_3Sb_5, Phys. Rev. Res. **5**, L012017 (2023).

[68] Heqiu Li, Xiaoyu Liu, Yong Baek Kim, and Hae-Young Kee, Origin of π-shifted three-dimensional charge density waves in the kagomé metal AV_3Sb_5 $(a = \mathrm{Cs}, \mathrm{Rb}, \mathrm{K})$, Phys. Rev. B **108**, 075102 (2023).

[69] Tian Le, Zhiming Pan, Zhuokai Xu, Jinjin Liu, Jialu Wang, Zhefeng Lou, Zhiwei Wang, Yugui Yao, Congjun Wu, and Xiao Lin, Evidence for chiral superconductivity in kagome superconductor CsV_3Sb_5, arXiv:2309.00264.

[70] Maxim Wenzel, Alexander A. Tsirlin, Francesco Capitani, Yuk T. Chan, Brenden R. Ortiz, Stephen D. Wilson, Martin Dressel, and Ece Uykur, Pressure evolution of electron dynamics in the superconducting kagome metal CsV_3Sb_5, npj Quantum Mater. **8**, 45 (2023).

[71] Harley D Scammell, Julian Ingham, Tommy Li, and Oleg P. Sushkov, Chiral excitonic order from twofold Van Hove singularities in kagome metals, Nat. Commun. **14**, 605 (2023).

[72] Alexander A. Tsirlin, Brenden R. Ortiz, Martin Dressel, Stephen D. Wilson, Stephan Winnerl, and Ece Uykur, Effect of nonhydrostatic pressure on the superconducting kagome metal CsV_3Sb_5, Phys. Rev. B **107**, 174107 (2023).

[73] See Supplemental Materials at http://link.aps.org/supplemental/10.1103/PhysRevLett.132.146501 for details on symmetry constraints on the effective Hamiltonian, and the discussion on Ginzburg-Landau analysis.